Evidence for seasonality in early Eocene high latitude sea-surface temperatures

Andrew Davies*[1,2], Stephen Hunter[2], Benjamin Gréselle[1], Alan M. Haywood[2], Chris Robson[1]

[1]Halliburton, 97 Jubilee Avenue, Milton Park, Abingdon, UK

[2]University of Leeds, School of Earth and Environment, Leeds, UK

*corresponding author: Andrew.davies@halliburton.com

Abstract

Specific challenges still exist in our understanding of past greenhouse climate states. Whilst climate model simulations using atmospheric CO_2 concentrations consistent with proxy estimates broadly align with lower latitude proxy temperature estimates, they struggle to reproduce the warming implied by proxies at higher latitudes, especially in the marine realm. This inconsistency has often led to the conclusion that climate models are insufficiently sensitive. Here, we analyse the distribution of photozoan and heterozoan carbonates, which provide important constraints for latitudinal sea surface temperature (SST) gradients, to assess data/model mismatches for the early Eocene Climatic Optimum. The carbonate facies distribution is compared against quantitative geochemical proxy temperature estimates ($\delta^{18}O$, Mg/Ca, clumped isotopes and TEX_{86}) and a new HadCM3L climate simulation. Good correspondence exists between the simulated cold-month SSTs and photozoan carbonates, indicating HadCM3L is effectively reconstructing meridional temperature gradients into mid-latitudes. Whilst there is good agreement between simulated mean annual SSTs and geochemical proxy estimates in low latitudes, the δ18O, Mg/Ca and TEX_{86} estimates instead align with warm-month SSTs at higher latitudes. In light of the carbonate facies evidence, and consistency between our simulation and available terrestrial proxy temperature estimates, this study supports previous claims that a warm season bias exists in many middle and high latitude SST estimates. This helps resolve the discrepancy between climate simulations and marine proxies and shows that climate models and data might be more closely aligned than is

appreciated. Further, we demonstrate that simple, and widely available, proxies can play a fundamental role in contextualising wider paleoclimate uncertainties.

1. Introduction

Since the early 1980s, numerical models of the climate system have been used to explore and better understand the climate evolution of our planet. During that time, the spatial resolution of models has increased, and their complexity has grown, fostering an ever-closer working relationship between modellers and geoscientists. Given the obvious potential relevance to future anthropogenic climate change, warm, high CO_2 climate states have become a particular focus. Such studies have demonstrated that whilst models are capable of simulating many of the large-scale features of past high CO_2 time periods (e.g. Lunt et al., 2012), comparisons with geological proxy data highlight specific challenges to our understanding of these greenhouse worlds remain. Whilst climate model simulations, conducted using atmospheric CO_2 concentrations consistent with proxy estimates, broadly align with proxy temperature estimates at lower latitudes, they are generally unable to reproduce the warming implied at higher latitudes (e.g. see figure 5 of Evans et al., 2018). This phenomenon is particularly well expressed in the marine realm with sea surface temperature (SST) proxy estimates generally indicating a greater magnitude of warming than suggested by terrestrial proxies (e.g. Huber and Caballero, 2011; Inglis et al., 2017). The data/model mismatches have often been attributed to inadequacies in climate models (e.g. Tierney et al., 2017; Evans et al., 2018), fuelling research into the physical parameterisations of climate models in order to generate warmer simulations (e.g. Sagoo et al., 2013; Upchurch et al., 2015) aligned with proxy temperature estimates (e.g. see figure 5 of Evans et al., 2018). Whilst these efforts are entirely appropriate, further research is also required to resolve some fundamental uncertainties that exist in some of the most commonly used paleotemperature proxies, including calibration issues (e.g. Ho and Laepple, 2016; Bernard et al., 2017) and the potential for a seasonal bias (e.g. Bijl et al., 2009; Hollis et al., 2012; Schouten et al., 2013).

Given these uncertainties, it can be challenging to conclude where the cause of data/model mismatches actually lies, and there is a potential risk of using circular reasoning to justify modifications to the physical representation of climate processes in models in the absence of actual observations. Numerous studies have explored data/model mismatches utilising a multi-proxy approach; however, to date, these have largely been confined to geochemical proxy methods (such as $\delta^{18}O$, TEX_{86} and Mg/Ca), particularly in the marine realm (e.g. Hollis et al., 2012; Lunt et al., 2012). A range of simpler proxies consisting of climatically sensitive sedimentary facies and their constituents also exist and, although used in early studies (Adams et al., 1990), remain underutilised. Whilst these proxies do not provide absolute temperature estimates, they can provide important constraints to determine if conditions were above or below certain temperature thresholds and provide independent evidence for the nature of past latitudinal SST gradients. Being abundantly available, they can therefore provide robust contextual control to help assess the cause of data/model mismatches. Here, a global database of geochemical and simpler proxies, in the form of different carbonate facies, is presented for the 53–50 Ma early Eocene climatic optimum (EECO) greenhouse period, along with a new climate simulation using the Hadley Centre Coupled Climate Model Version 3 (HadCM3L). The model results are compared to carbonate facies data in an effort to independently determine the early Eocene latitudinal SST gradient and critically assess the nature of data/model mismatches in a holistic way.

2. The early Eocene climate

Available lines of evidence indicate that the early Eocene climate was in a greenhouse state, with the EECO marking the culmination of a late Paleocene-early Eocene long-term warming trend. Concentrations of atmospheric CO_2 during the EECO were greater than the modern with proxy-based estimates from a variety of techniques generally indicating levels were between 1.5 to 10 times pre-industrial levels (see Supplemental files for details). Previous climate modelling studies have often used values within this range, although some have employed values beyond the upper limits indicated by proxies in order to assess the importance of CO_2 forcing uncertainty on the simulation (e.g. Huber and Caballero, 2011; Hollis et al., 2012; Keery et al., 2018). The importance of the long-term geological carbon cycle in forcing past greenhouse climate states was clearly demonstrated in an Early Cretaceous to Eocene ensemble study which established that global mean annual temperatures are largely unaffected by time dependent solar and paleogeographic forcings (Lunt et al., 2016). Other model studies have demonstrated that CO_2 accounts for over 90% of the variance in a range of temperature parameters (Keery et al., 2018). During the early Eocene, surface temperatures were elevated at all latitudes, with higher latitudes showing the largest surface temperature response (e.g. Lunt et al., 2012). The term 'equable' has been used to describe such climate states, characterized by a reduced equator-to-pole temperature gradient with warm, ice-free polar regions. The equable climate characteristics are well expressed in early Eocene marine geochemical proxies which indicate that whilst tropical SSTs were moderately (3-8°C) warmer than present (Evans et al., 2018), there was a marked increase (10–25°C) in mid to high latitude SSTs (Bijl et al., 2009; Cramwinckel et al., 2018) (see Supplemental files for details)

Despite attempts to simulate equable climate conditions, persistent data–model inconsistencies remain, particularly in high latitudes, which has been termed the 'equable climate problem' (Sloan and Barron, 1990). The collapse of latitudinal temperature gradients is difficult to reconcile with the climate dynamics that underpin climate models (e.g. Lunt et al., 2012) and as a result, most early Eocene climate simulations are inconsistent with the full range of proxy data (Lunt et al., 2012, 2013; Evans et al., 2018). Climate model simulations can generate global air temperature distributions in broad agreement with the early Eocene terrestrial proxy temperature estimates (Huber and Caballero, 2011), but challenges remain in simulating SST gradients using atmospheric CO_2 concentrations consistent with proxy constraint. This is in part related to marine proxies generally indicating warming of greater magnitude than terrestrial proxies (Huber and Caballero, 2011; Inglis et al., 2017). Unsurprisingly, warmer surface conditions appear to have led to a general enhancement in the hydrological cycle (Carmichael et al., 2018) with a warmer atmosphere also having an increased moisture carrying capacity following the Clausius–Clapeyron relationship (Lunt et al., 2012). The resulting differences in cloud properties may be an important factor behind the data/model discrepancies of equable climates (Kiehl and Shields, 2013; Upchurch et al., 2015) and models with perturbed physics parameters have provided simulations that are more consistent with the range of proxies (e.g. Sagoo et al., 2013). Despite this promising line of investigation, data/ model comparisons are complicated by the presence of a number of sources of uncertainty in established paleothermometry techniques that require consideration before definitive conclusions can be made on the cause of data/model discrepancies.

It is well established that $\delta^{18}O$ temperatures are commonly affected by diagenetic alteration (Pearson et al., 2001) for which the practice of picking "glassy" specimens was developed. However, it has been recently demonstrated that the $\delta^{18}O$ composition of calcite may undergo alteration through diffusion during burial without any observable changes to the fossil ultrastructure (Bernard et al., 2017). This diffusive isotope re-equilibration influences the $\delta^{18}O$ composition of the fossils that formed in cold waters, potentially causing overestimation of ocean temperatures at high latitudes. The physiological imprinting of geochemical signals (or vital effects) are another source of uncertainty in $\delta^{18}O$ temperature estimates (Hermoso et al., 2014) and both $\delta^{18}O$ and Mg/Ca are highly sensitive to secular variations in salinity and seawater chemistry (e.g. Evans et al., 2016). TEX_{86} is associated with calibration complications (Tierney and Tingley, 2014; Ho and Laepple, 2016) and non-thermal factors may also influence the glycerol dialkyl glycerol tetraether (GDGT) signal (e.g. Elling et al., 2015). It has also been demonstrated that $\delta^{18}O$, Mg/Ca and TEX_{86} derived SST estimates could all be seasonally biased to summer temperatures at mid to high latitudes (Hollis et al., 2012). While some of these uncertainties may help explain the inconsistencies between climate simulations and proxy data, the debate has recently been reinvigorated through new peat-based branched glycerol dialkyl glycerol tetraether (brGDGT) data that indicate the terrestrial realm may have been much warmer than previously thought during the early Paleogene (Naafs et al., 2018). Additional lines of evidence are therefore needed to help critically assess the nature of the data/model mismatches characteristic of equable climates such as the early Eocene.

3. Carbonate facies as climate proxies

Temperature strongly affects many biological processes within the marine environment and the large-scale distribution of various carbonate producing organisms is clearly related to ocean temperature. Shallow-marine, benthic carbonates have been classified into “photozoan” or “heterozoan” associations (James, 1997), that are produced in tropical or cool-water “factories” (sensu Schlager, 2003). A characteristic feature of photozoan, or tropical, carbonates is the presence of photosymbiont-bearing invertebrates, such as zooxanthellate coral and large benthic foraminifera (LBF). The modern distribution of these organisms is clearly temperature controlled with coral-bearing photozoan carbonate assemblages constrained to tropical/subtropical environments where SSTs remain above 18°C in the coldest month (Fig 1). However, some LBF are able to tolerate a wider range of temperatures (Fig. 1), with most species found in areas where cold month ocean temperatures do not fall below 15°C (Langer and Hottinger, 2000), although some are able to exist in regions where winter temperatures fall as low as 14°C (Langer and Hottinger, 2000; Beavington-Penney and Racey, 2004). Temperature has a crucial role in controlling the geographical distribution of photozoan carbonate assemblages as it influences the energy required to generate skeletal carbonate by impacting the solubility of CO_2 and the saturation of $CaCO_3$ in seawater (Mutti and Hallock, 2003). Aragonite precipitation, characteristic of zooxanthellate corals and calcareous green algae, is most advantageous in warm waters, supersaturated with $CaCO_3$. Calcite-secreting organisms are favoured in cooler waters, where greater energy is required to precipitate aragonite (Hallock, 2001). Lower temperatures also inhibit the ability of the symbiotic algae, present within both corals and LBF, to photosynthesise, leading to a potential net loss of carbon transferred from the algae to the host (Hollaus and Hottinger, 1997; Kemp et al., 2011). Whilst temperature plays a crucial role in photozoan carbonate distribution, other factors such as light intensity, trophic level, and pH are also important considerations. In contrast, heterozoan carbonates are comprised of heterotrophic invertebrates (such as small benthic foraminifera, molluscs, and bryozoans). Red calcareous algae can be abundant in both heterozoan and photozoan assemblages. Heterozoan assemblages can occur within a wide spectrum of trophic levels and climatic zones but are generally swamped by rapidly growing photozoan material in tropical environments. Heterozoan assemblages are therefore typical, but not exclusively reflective, of temperate to polar environments where summer SSTs remain cooler than 24°C (Michel et al., 2018).

4. Materials and methods

4.1 Climate proxies

A database of benthic carbonate assemblages from 56 sites (see Supplemental files for details) was collated and characterised as either “photozoan” or “heterozoan” following the definition of (James, 1997). To address uncertainty in our classification we also applied a confidence rating. A high confidence was designated if the section was known to contain photosymbiont bearing invertebrates (e.g. corals and LBF) or green calcareous algae. Due to the propensity of photozoan corals to be hermatypic, rimmed platforms and their associated lagoons are also diagnostic facies associated with photozoan carbonates. Photozoan carbonates may also be associated with coastal sabkhas, such as those present along the modern Arabian margin of the Persian Gulf. We therefore also classified carbonates known to have facies associations with evaporites, lagoons, and reefs as high confidence. A lone facies association, such as the presence of a reef, is suggestive of photozoan carbonates, but is not definitive, and so in these instances a low confidence designation was assigned (see Supplemental files for additional details). As ocean temperature generally decrease with depth, only those sections deposited in shallow marine settings were considered when collating the carbonate proxies to ensure a fair reflection of SST. As a result of the quality of the temporal control in these sections, any deposit that could be constrained to the Ypresian or early Eocene was utilised. However, as the poleward extent of photozoan carbonates is controlled by cold month temperatures, the widest latitudinal distribution can be expected during peak warmth, when high latitude winter SSTs would be at their highest. Therefore, these data should still provide robust constraint for the EECO. As with other paleotemperature proxies, we assume that the strong correlation between the distribution of carbonate facies and temperature observed in the modern was the same during the early Eocene.

Additionally, quantitative geochemical marine proxies (TEX_{86}, $\delta^{18}O$, Mg/Ca, and clumped isotope data) were collated from 22 sites (Fig. 2) and screened to ensure only those data matching the biostratigraphic calibration of the EECO were used (see Supplemental files for details). The highest and lowest temperature values for the EECO interval were captured and the values were taken as published by the authors; no attempt was made to recalculate the values. Quantitative terrestrial temperature proxies were also obtained from a recent early Paleogene synthesis (Naafs et al., 2018), comprising 55 temperature estimates derived from leaf physiognomy, lignite GDGT, mammal $\delta^{18}O$, MBT/CBT (the methylation of branched tetraether and cyclization of branched tetraethers), paleosols and nearest living relatives data (see Supplemental files). In a similar manner to the marine proxy temperatures, the highest and lowest temperature values for the EECO interval were captured and the temperature values were taken as published by the authors.

4.2 Climate simulation

The HadCM3L General Circulation Model was used to generate a new EECO simulation (see Supplemental files for additional details). We incorporated the land surface scheme MOSES 2.1 (Essery et al., 2003) with a land surface consisting of lakes and homogenous shrub. Atmospheric CO_2 concentration was prescribed at 1200 ppm, consistent with the most recent boron isotope data (Anagnostou et al., 2016). Other atmospheric constituents were held at preindustrial levels. The EECO tectonic configuration, gross depositional environments and resulting paleo digital elevation model (PDEM) that underpins this study were created by Halliburton Neftex® Insights using a modified version of the approach of Vérard et al. (2015) to include a wider range of input data. The PDEM, land sea mask, and lake fields were regridded to model resolution using an area-weighted algorithm. Model specific smoothing was applied to the bathymetry and hand edits applied where the land sea mask was unsatisfactory. A model resolution river drainage model was generated that is internally consistent with the PDEM and known river outlets. To address the paleolatitudinal uncertainty of the proxy data, the range of possible paleo-coordinates for each was captured from 8 different plate tectonic models using PaleoGIS software and the paleolatitude calculator of van Hinsbergen et al. (2015), ensuring the uncertainty estimates consider both hotspot and paleomagnetic derived reference frames (see Supplemental files). Latitudinal temperature gradients were extracted from the time-averaged simulation results, and data were binned by latitude using the model grid cells. Zonal mean, maximum and minimum values were obtained for the annual mean, cold-month mean (CMM) and warm-month mean (WMM) SST, and air temperature.

5. Results

5.1. Simulation and marine proxy data comparison

Our simulation achieved a satisfactory state of equilibrium within the atmosphere and ocean with a 1.5M global mean annual temperature of 24.28°C trending at -0.03°C century^{-1}. The simulation has a globally-integrated Top of the Atmosphere Radiative (TOA) imbalance of 0.12 W m^{-2} with a potential temperature trend in the top 200m of the water column of -0.015°C century^{-1} (see Supplemental files for additional information). Our simulation therefore has a climatological mean TOA imbalance that compares favourably with the 0.06 W m^{-2} imbalance from the model's pre-industrial experiment and is well within the tolerance suggested by Lunt et al., (2017) (see Supplemental files for details).

There is good agreement between the geographic distribution of the different photozoan assemblages and the CMM SSTs generated by this simulation (Fig. 3). 51 out of the 53 pure photozoan carbonate sites are located where simulated CMM SSTs do not fall below 14°C (Figs. 3), the temperature tolerance of modern forms (Beavington-Penney and Racey, 2004). However, the two photozoan sites that occur outside of the 14°C temperature threshold (Inal and Hampshire Basin) are consistent with the simulation when the paleolatitudinal uncertainty and zonal range are considered (Fig. 4). LBF are able to tolerate cooler conditions that is typical for other photozoan assemblages, and when sites comprised solely of LBF are excluded, all other sites occur where simulated CMM SSTs remain above 18°C (Figs. 3 and 4), consistent with modern temperature tolerances. Only a small selection of heterozoan carbonates could be identified, and all occur in the southern hemisphere. In Victoria, Australia, the Dilwyn Formation contains solitary scleractinian corals within a heterozoan assemblage that is interpreted to have been deposited in a shoreface or coastal environment (Stilwell, 2003) at 62-55° S. This sole pure heterozoan site was deposited in a paleolatitude (62-55°S) where CMM SSTs do not or are unlikely to reach the 14°C threshold for photozoans (Beavington-Penney and Racey, 2004) and simulated WMM SSTs remain below 24°C, where heterozoans more typically occur today

(Michel et al., 2018). Deposited in slightly lower paleolatitudes (57-51° S), the basal unit of the Matanginui Limestone Member on the Chatham Islands, New Zealand, is a dominantly bryozoan packstone to grainstone that is typical of an heterozoan assemblage (James et al., 2011). The upper unit contains bryozoan with locally abundant LBF and echinoids. The unit is interpreted to have been deposited in a neritic environment within the photic zone (James et al., 2011). The underlying early Eocene and overlying middle to late Eocene carbonates are wholly heterozoan. The Chatham Island succession lies in an area where simulated CMM SSTs fall just below the 14°C threshold for photozoans (Fig. 3), although when the paleolatitudinal uncertainty and zonal range are considered, the climate simulation is consistent with photozoan carbonate accumulation at this site (Fig. 4).

A close correspondence between the simulated latitudinally binned mean annual SSTs and a range of estimates from low latitude sites (>30°) is evident (Fig. 4), including those derived from TEX_{86} (Tanzania and ODP Site 959 and 929), $\delta^{18}O$ (Tanzania), Mg/Ca (ODP Site 865) and clumped isotope analysis (Kutch, India). Simulated SSTs are consistent with mid latitudes (30-60°) estimates from TEX_{86} (Well 10, Wilson Lake, South Dover Bridge, and Hatchetigbee), and clumped isotopes (Hatchetigbee, Kester Borehole, and Paris Basin). However, a number of proxy estimates are elevated compared to the simulated mean annual SSTs, including those derived from TEX_{86} (U1356A, ODP Site 1172D and Waipara), $\delta^{18}O$ (Waipara, Belgium Basin), and Mg/Ca (Tawanui, Tora, Waipara, Hampden, and ODP Site 1172D), which align more closely with WMM ranges. In high latitudes, there is some agreement between our simulation and $\delta^{18}O$ estimates from ODP Site 690, whilst estimates from ODP Site 738 and DSDP 277 are elevated compared to the mean. However, these high latitudes estimates may not be robust as the planktic foraminifera at ODP Sites 690 and 738, and DSPS Site 277 appear to be variably affected by seafloor diagenesis (Hollis et al., 2012). High latitude TEX_{86} estimates from IODP Site 302-4A are also elevated compared to the simulated mean annual SSTs and again align with simulated WMM SSTs.

5.2. Simulation and terrestrial proxy data comparison

In general, there is a high level of agreement between our simulation and quantitative terrestrial proxy temperature estimates (Fig. 5). Simulated temperatures are consistent with all mammal-derived $\delta^{18}O$

temperature estimates from mid to high paleolatitudes sites. In mid latitudes there is also good agreement with temperature estimates derived from nearest living relative, leaf physiognomy, and MBT/CBT in both hemispheres. However, our simulation is inconsistent with lignite GDGT temperature estimates (Otaio and Schoeningen), which are warmer than simulated temperatures in both hemispheres. There is agreement with some nearest living relative, MBT/CBT and leaf physiognomy data in high latitudes, but discrepancies are present. Estimates from nearest living relative data from Faddeevsky Island in high northern latitudes are warmer than our simulated temperatures, as are some estimates from nearest living relative data (Lowana Road, Dean's Marsh and Wilkesland), MBT/CBT (IODP sites U1356 and 1172), and leaf physiognomy (Brandy Creek and Hotham Heights, Australia) in high southern latitudes. There is relatively poor correlation with the sparse low latitude proxy temperature estimates, including those derived from paleosols (Argentina), lignite GDGT (Khadsaliya, Matanomadh and Panandhro, India), and leaf physiognomy (Gurha, India) which are all cooler than simulated temperatures.

6. Discussion

6.1. Temperature control on carbonate proxies

Temperature is not the only control on carbonate facies distribution, and these other factors need consideration. Light intensity is an important ecological control for photozoan assemblages due to their dependency on photosynthesis. However, studies on extant species of LBF and photozoan corals demonstrate that they can thrive in low-light conditions (Anthony and Hoegh-Guldberg, 2003; Hohenegger et al., 2000), making it unlikely that the early Eocene geographic distribution can be explained by light intensity. Trophic levels are another important control on modern photozoan assemblages and increased nutrient levels, resulting from elevated fluvial runoff or upwelling, could explain the restricted paleolatitudinal extent of early Eocene photozoan. However, the ability of LBF to tolerate elevated trophic levels has been implicated in their dominance during the EECO (Scheibner and Speijer, 2008). This hypothesis is supported by the presence of LBF in early Eocene clastic-dominated sequences, such as the UK, and is further supported by studies on modern LBF which demonstrate they are resilient to increased nitrate levels (Prazeres et al., 2017). Surface ocean acidification associated with elevated atmospheric CO_2, is also unlikely to have an impact on the observed distribution of photozoan carbonates as surface ocean pH is unlikely to have has much latitudinal variability and may have even been more alkaline at higher latitudes (Gutjahr et al., 2017). In light of these lines of evidence and following conclusions of Schlager (2003), we conclude that temperature has a dominant role in controlling latitudinal photozoan distribution during the early Eocene.

Despite this, it is important to consider whether the modern temperature thresholds used in this study are likely to be valid for the early Eocene. In light of the metabolic factors controlling the minimum temperature threshold of the various photozoans (see section 3), we conclude that it is unlikely that early Eocene forms would be able to tolerate cooler conditions than modern forms. However, we have employed the coldest thresholds of modern forms that could introduce a bias into our results. Independent support for our approach does exist however, in the clumped isotope temperature data from northern middle latitudes (Kester borehole and Paris Basin), close to the northerly extent of LBF (Fig. 4). These data likely reflect mean annual SST as they either originate from LBF, which calcify at a constant rate in locations characterized by a large seasonal cycle (e.g. Evans et al., 2018), or are pooled from multiple bivalve shells encompassing growth bands from different seasons (Keating-Bitonti et al., 2011). These data provide mean annual SST estimates of 18.5 – 20°C ± ~2.5 °C (Evans et al., 2018) and therefore support the use of the modern (14°C), rather than a warmer, CMM threshold for LBF. It is also evident that early Eocene photozoan corals were deposited across a narrower latitudinal range then LBF, suggesting they were more sensitive to CMM temperatures, consistent with modern observations. When combined with the clumped isotope temperature data from the Kester borehole and Paris Basin, this supports our use of the modern 18°C CMM threshold for photozoan corals.

6.2. Implications for early Eocene ocean temperatures

The excellent agreement between the simulated CMM SSTs and the photozoan/heterozoan distribution suggests that HadCM3L is effectively reconstructing meridional cold-season conditions using modest levels of atmospheric CO_2. This is further supported by good agreement with the geochemical proxies in low to mid latitudes, especially in the northern hemisphere. Although the climate simulation is consistent with photozoan carbonate accumulation on the Chatham Islands given the paleolatitudinal uncertainty and zonal temperature ranges, the alternating heterozoan/photozoan assemblages deposited there might be better explained by the impact of orbital forcing on CMM conditions. Modern orbital parameters were used in this study, but photozoans may have been periodically deposited on the Chatham Islands when orbital parameters favoured warmer southern hemisphere winters, although changes in another forcing agent, such as atmospheric CO_2, or in relative water depth cannot be ruled out. In combination, our observations leave two scenarios to explain the mismatch with TEX_{86}, Mg/Ca, and $\delta^{18}O$ temperature estimates at high and some middle latitude sites. The first scenario is that the proxy estimates exclusively record the mean annual SST, and despite providing robust CMM SSTs, HadCM3L is underestimating the mean and hence WMM temperature. Whilst we cannot definitively rule this possibility out, it appears unlikely and is difficult to reconcile with the temperature gradient implied by the latitudinal ranges of LBF and photozoan corals. There is also some support for the WMM simulation in the limited EECO heterozoan data, which are located where WMM SSTs remain below 24°C, conditions where heterozoan carbonates more typically occur today.

The alternative scenario is that some mid to high latitude SST estimates are seasonally biased, as suggested by a number of other workers (e.g. Sluijs et al., 2006; Bijl et al., 2009; Davies et al., 2009; Eberle et al., 2010; Hollis et al., 2012; Pancost et al., 2013) and that the seasonal bias becomes increasingly amplified at higher latitudes. Evidence for a seasonal bias in Mg/Ca and $\delta^{18}O$ is supported by modern studies in the Southern Ocean, which demonstrate surface-dwelling planktic foraminiferal production peaks in late spring or summer (King and Howard, 2005). Thaumarchaeota, the source of the TEX_{86} signal, most likely reached the seafloor within faecal pellets, creating a strong link with grazing. In high latitudes, grazing intensity is likely to be strongly seasonal, with more intense grazing during the ecologically favourable summer period. This is supported by modern studies offshore eastern New Zealand, which demonstrate the greatest flux of particulate organic matter is in mid-to late-spring (Nodder and Northcote, 2001). In lower latitudes, where seasonality is reduced, this bias likely diminishes and estimates here are more likely to reflect mean annual conditions. A key piece of support for the presence of a seasonal bias is that our photozoan data and simulation are consistent with temperature estimates derived from clumped isotope data in both the tropics (Kutch, India) and in mid latitudes (Hatchetigbee, Kester Borehole and Paris Basin), which are likely to reflect mean annual SST (Evans et al., 2018). If a warm-month seasonal bias is acknowledged in mid to high latitude proxy temperature estimates from TEX_{86} (IODP sites U1356A and 302-4A, ODP Site 1172D, Waipara and Well 10), $\delta^{18}O$ (Waipara, Belgium Basin), and Mg/Ca (Tawanui, Tora, Waipara, Hampden and DSDP Site 277), then marine proxies demonstrate good agreement with simulated temperatures, although the southern hemisphere sites remain on the upper end of the zonal range. Future work to explore the impact of differing orbital parameters and higher atmospheric CO_2 concentrations on simulated temperatures may help further improve the correlation in this area, and the generation of clumped isotope temperature estimates in the southern middle to high latitudes will help evaluate the claim of a seasonal bias in the existing proxy estimates. Despite this, we feel the photozoan distribution provides robust evidence for a seasonal bias. There is support for our use of the modern CMM SST thresholds for photozoan corals and LBF (see section 6.1), but even if higher thresholds are used (e.g. 20°C and 16°C), the different latitudinal ranges of LBF and photozoan corals implies the presence of a latitudinal thermal gradient that is difficult to reconcile with high latitude tropical mean annual SSTs. If our conclusions are correct, it follows that changes to the physical parameterisation of climate models may not in fact be needed to obtain a closer correspondence between simulations and proxy data.

6.3. Implications for early Eocene air temperatures

Our conclusion that HadCM3L is effectively reconstructing meridional temperature gradients is further supported by the close agreement between our simulated air temperatures and the bulk of the terrestrial proxy temperature estimates (Fig. 5). However, inconsistencies are present, and it is important to understand to what these may relate. Firstly, there are mismatches between the paleosol temperatures of ~10°C in southern hemisphere mid latitudes (~30°). These temperatures appear anomalously cold even for today and have been previously related to either a cold-month bias or lapse rate effects (Naafs et al., 2018). Additionally, there is disagreement with MBT/CBT-based temperatures in southern high latitudes from IODP site 1172, IODP Site U1356 and Waipara. The MBT/CBT approach utilises bacterial derived brGDGTs to estimate air temperature. The disagreement noted here occurs with data derived from marine sediments where it appears that the reconstruction of meaningful terrestrial estimates is complicated, because the signal can be contaminated with brGDGTs generated in the water column, in the sediment column or within the river itself (Sinninghe Damsté, 2016). The brGDGT signal may also suffer from a warm season bias (Bijl et al., 2013) and the signals might be further complicated due to a blending of temperature signals resulting from large drainage basins and co-eluting compounds (De Jonge et al., 2014).

Discrepancies are evident with the paleobotanical nearest living relative data from high paleolatitude, (81.7 - 77.8°N) sites in Russia. However, the EECO high latitudes represent a true non-analogue environment with warm summer temperatures accompanied by 24 hours of sunlight daily. This might have allowed some plants to live beyond their modern ecological tolerances; for example, the occurrence of palms is not simply prevented by low temperature (Gatti et al., 2008). The range of the palm Trachycarpus fortune in Asia is limited by a combination of winter temperatures and a subordinate effect of cumulative growing season energy, with the range limit being imposed by frost damage to leaves that cannot be compensated by biomass production in the following growing season (Walther et al., 2007). Therefore, the effect of cold winter temperatures might have been offset by prolific summer growing seasons in the EECO high latitudes. As such, the cold temperature tolerance of Eocene polar palms might have differed markedly from the modern. Indeed, Read and Francis (1992) suggest that cool winter temperatures may actually be necessary for high latitude forests to have developed, as respiration induced carbon loss increases with temperature. This difference in temperature tolerance may in part also explain the discrepancy between our simulation and nearest living relative derived mean annual air temperatures from Australia (65-55°S) and Antarctica (62-58°S).

Lastly, there are mismatches with a temperature estimate from newly calibrated peat-based brGDGT data (Naafs et al., 2018). The brGDGT proxy reaches saturation at 29.1°C and therefore the mismatches near the equator can be discounted as these likely represent minimum temperatures (Naafs et al., 2018). However, the mismatch with brGDGT data from mid latitude sites in present day New Zealand and Germany are more difficult to explain (Fig. 5). It is known that brGDGT production is seasonally influenced and a warm-season bias is present in some modern soils (Wang et al., 2018), although it appears that the brGDGT distribution in peat is dominated by production below the water table where the seasonal temperature cycle is muted (Naafs et al., 2017). However, there are uncertainties in the interpretation of brGDGT temperature estimates as information on the ecology of the bacterial producers of brGDGTs is scarce with most producers of these lipids unidentified (Naafs et al., 2017). The type of vegetation growing in the soil has also been shown to influence the brGDGT temperature estimates (Liang et al., 2019) and it is also possible that the signal could be influenced by in-situ production of brGDGT at depths during burial where temperature exceeds the surface conditions. This possibility could be explored by investigating brGDGT data from a single stratigraphic unit with a variable burial history and tight chronological control against thermal maturity indicators. As the brGDGT temperature estimates are generally warmer than other air temperature proxies at similar latitudes, another possibility is that they record the extreme end of the zonal temperature range (Douglas et al., 2014; Naafs et al., 2018), beyond the resolution of HadCM3L.

7. Conclusions

This study demonstrates an excellent correspondence between simulated cold-month SSTs and photozoan carbonate distribution, indicating HadCM3L is effectively reconstructing meridional EECO temperature gradients into mid-latitudes using moderate levels of atmospheric CO_2. The carbonate facies distribution is inconsistent with many of the middle and high latitude geochemical temperature estimates recording mean annual SSTs. This work therefore adds to a growing body of literature that suggests a seasonal bias may be implicit in a number of previously reported deep time data/model mismatches, helping to explain the flat meridional gradient some geochemical proxies generate during periods of global warmth. Further, we demonstrate that simple marine proxies can help resolve some long-standing inconsistencies between geochemical marine proxies and climate simulations. Being widely available, these simpler proxies have a key role in contextualising uncertainties associated with quantitative geochemical climate proxies and further research is suggested to validate this approach on other equable climate states. The technique could also be refined in future by assessing the distribution of additional features of the photozoan assemblages (e.g. calcareous green algae and non-biogenic precipitates) and assessing individual taxonomic groups. One remaining challenge for the EECO is the correlation with geochemical proxies in southern middle latitudes that are on the upper limit of the zonal range in our simulation. Additional climate simulations to explore the impact of differing orbital parameters and atmospheric CO_2 concentrations on simulated CMM SSTs are required.

Our work provides a case study for determining the cause of data/model mismatches in a holistic way, providing a framework to allow refinements to quantitative proxy temperature estimates in future. It cannot be assumed that quantitative proxy temperature estimates faithfully represent an annual mean temperature at all latitudes and the full seasonal signal, including zonal ranges, should be extracted from climate simulations for the purposes of data/model comparison. Given the scope of geological uncertainties, all lines of evidence should be explored using a holistic multi-proxy assessment before definitive statements on the magnitude of previous warmth, or model performance, are made.

Acknowledgements

The authors thank Steve Bohaty, Bette Otto-Bliesner, Frans van Buchem, Mike Simmons and three anonymous reviewers for their useful remarks that helped to improve the clarity of our paper. We also thank Halliburton for permission to publish this work.

References

Adams, C.G., Lee, D.E., Rosen, B.R., 1990. Conflicting isotopic and biotic evidence for tropical sea-surface temperatures during the Tertiary. Palaeogeogr. Palaeoclimatol. Palaeoecol., Pacific

Neogene event stratigraphy and paleoceanographic history 77, 289–313. https://doi.org/10.1016/0031-0182(90)90182-7

Anagnostou, E., John, E.H., Edgar, K.M., Foster, G.L., Ridgwell, A., Inglis, G.N., Pancost, R.D., Lunt, D.J., Pearson, P.N., 2016. Changing atmospheric CO_2 concentration was the primary driver of early Cenozoic climate. Nature 533, 380–384. https://doi.org/10.1038/nature17423

Anthony, K.R.N., Hoegh-Guldberg, O., 2003. Variation in coral photosynthesis, respiration and growth characteristics in contrasting light microhabitats: an analogue to plants in forest gaps and understoreys? Funct. Ecol. 17, 246–259. https://doi.org/10.1046/j.1365-2435.2003.00731.x

Beavington-Penney, S.J., Racey, A., 2004. Ecology of extant nummulitids and other larger benthic foraminifera: applications in palaeoenvironmental analysis. Earth-Sci. Rev. 67, 219–265. https://doi.org/10.1016/j.earscirev.2004.02.005

Bernard, S., Daval, D., Ackerer, P., Pont, S., Meibom, A., 2017. Burial-induced oxygen-isotope re-equilibration of fossil foraminifera explains ocean paleotemperature paradoxes. Nat. Commun. 8, 1134. https://doi.org/10.1038/s41467-017-01225-9

Bijl, P.K., Bendle, J.A.P., Bohaty, S.M., Pross, J., Schouten, S., Tauxe, L., Stickley, C.E., McKay, R.M., Röhl, U., Olney, M., Sluijs, A., Escutia, C., Brinkhuis, H., Scientists, E. 318, 2013. Eocene cooling linked to early flow across the Tasmanian Gateway. Proc. Natl. Acad. Sci. 110, 9645–9650. https://doi.org/10.1073/pnas.1220872110

Bijl, P.K., Schouten, S., Sluijs, A., Reichart, G.-J., Zachos, J.C., Brinkhuis, H., 2009. Early Palaeogene temperature evolution of the southwest Pacific Ocean. Nature 461, 776–779. https://doi.org/10.1038/nature08399

Carmichael, M.J., Pancost, R.D., Lunt, D.J., 2018. Changes in the occurrence of extreme precipitation events at the Paleocene–Eocene thermal maximum. Earth Planet. Sci. Lett. 501, 24–36. https://doi.org/10.1016/j.epsl.2018.08.005

Cramwinckel, M.J., Huber, M., Kocken, I.J., Agnini, C., Bijl, P.K., Bohaty, S.M., Frieling, J., Goldner, A., Hilgen, F.J., Kip, E.L., Peterse, F., Ploeg, R. van der, Röhl, U., Schouten, S., Sluijs, A., 2018. Synchronous tropical and polar temperature evolution in the Eocene. Nature 559, 382. https://doi.org/10.1038/s41586-018-0272-2

Davies, A., Kemp, A.E.S., Pike, J., 2009. Late Cretaceous seasonal ocean variability from the Arctic. Nature 460, 254–258. https://doi.org/10.1038/nature08141

De Jonge, C., Hopmans, E.C., Zell, C.I., Kim, J.-H., Schouten, S., Sinninghe Damsté, J.S., 2014. Occurrence and abundance of 6-methyl branched glycerol dialkyl glycerol tetraethers in soils: Implications for palaeoclimate reconstruction. Geochim. Cosmochim. Acta 141, 97–112. https://doi.org/10.1016/j.gca.2014.06.013

Douglas, P.M.J., Affek, H.P., Ivany, L.C., Houben, A.J.P., Sijp, W.P., Sluijs, A., Schouten, S., Pagani, M., 2014. Pronounced zonal heterogeneity in Eocene southern high-latitude sea surface temperatures. Proc. Natl. Acad. Sci. 111, 6582–6587. https://doi.org/10.1073/pnas.1321441111

Eberle, J.J., Fricke, H.C., Humphrey, J.D., Hackett, L., Newbrey, M.G., Hutchison, J.H., 2010. Seasonal variability in Arctic temperatures during early Eocene time. Earth Planet. Sci. Lett. 296, 481–486. https://doi.org/10.1016/j.epsl.2010.06.005

Elling, F.J., Könneke, M., Mußmann, M., Greve, A., Hinrichs, K.-U., 2015. Influence of temperature, pH, and salinity on membrane lipid composition and TEX_{86} of marine planktonic thaumarchaeal isolates. Geochim. Cosmochim. Acta 171, 238–255. https://doi.org/10.1016/j.gca.2015.09.004

Essery, R.L.H., Best, M.J., Betts, R.A., Cox, P.M., Taylor, C.M., 2003. Explicit Representation of Subgrid Heterogeneity in a GCM Land Surface Scheme. J. Hydrometeorol. 4, 530–543. https://doi.org/10.1175/1525-7541(2003)004<0530:EROSHI>2.0.CO;2

Evans, D., Sagoo, N., Renema, W., Cotton, L.J., Müller, W., Todd, J.A., Saraswati, P.K., Stassen, P., Ziegler, M., Pearson, P.N., Valdes, P.J., Affek, H.P., 2018. Eocene greenhouse climate revealed by coupled clumped isotope-Mg/Ca thermometry. Proc. Natl. Acad. Sci. 115, 1174–1179. https://doi.org/10.1073/pnas.1714744115

Evans, D., Wade, B.S., Henehan, M., Erez, J., Müller, W., 2016. Revisiting carbonate chemistry controls on planktic foraminifera Mg / Ca: implications for sea surface temperature and hydrology shifts over the Paleocene–Eocene Thermal Maximum and Eocene–Oligocene transition. Clim. Past 12, 819–835. https://doi.org/10.5194/cp-12-819-2016

Gatti, M.G., Campanello, P.I., Montti, L.F., Goldstein, G., 2008. Frost resistance in the tropical palm Euterpe edulis and its pattern of distribution in the Atlantic Forest of Argentina. For. Ecol. Manag. 256, 633–640. https://doi.org/10.1016/j.foreco.2008.05.012

Gutjahr, M., Ridgwell, A., Sexton, P.F., Anagnostou, E., Pearson, P.N., Pälike, H., Norris, R.D., Thomas, E., Foster, G.L., 2017. Very large release of mostly volcanic carbon during the Palaeocene–Eocene Thermal Maximum. Nature 548, 573–577. https://doi.org/10.1038/nature23646

Hallock, P., 2001. Coral Reefs, Carbonate Sediments, Nutrients, and Global Change, in: Stanley, G.D. (Ed.), The History and Sedimentology of Ancient Reef Systems, Topics in Geobiology. Springer US, Boston, MA, pp. 387–427. https://doi.org/10.1007/978-1-4615-1219-6_11

Hermoso, M., Horner, T.J., Minoletti, F., Rickaby, R.E.M., 2014. Constraints on the vital effect in coccolithophore and dinoflagellate calcite by oxygen isotopic modification of seawater. Geochim. Cosmochim. Acta 141, 612–627. https://doi.org/10.1016/j.gca.2014.05.002

Ho, S.L., Laepple, T., 2016. Flat meridional temperature gradient in the early Eocene in the subsurface rather than surface ocean. Nat. Geosci. 9, 606–610. https://doi.org/10.1038/ngeo2763

Hohenegger, J., Yordanova, E., Hatta, A., 2000. Remarks on West Pacific Nummulitidae (Foraminifera). J. Foraminifer. Res. 30, 3–28. https://doi.org/10.2113/0300003

Hollaus, S.S., Hottinger, L., 1997. Temperature dependence of endosymbiotic relationships? Evidence from the depth range of Mediterranean Amphistegina lessonii (Foraminiferida) truncated by the thermocline. Eclogae Geol. Helvetiae 90, 591–597.

Hollis, C.J., Taylor, K.W.R., Handley, L., Pancost, R.D., Huber, M., Creech, J.B., Hines, B.R., Crouch, E.M., Morgans, H.E.G., Crampton, J.S., Gibbs, S., Pearson, P.N., Zachos, J.C., 2012. Early Paleogene temperature history of the Southwest Pacific Ocean: Reconciling proxies and models. Earth Planet. Sci. Lett. 349–350, 53–66. https://doi.org/10.1016/j.epsl.2012.06.024

Huber, M., Caballero, R., 2011. The early Eocene equable climate problem revisited. Clim. Past 7, 603–633. https://doi.org/10.5194/cp-7-603-2011

Inglis, G.N., Collinson, M.E., Riegel, W., Wilde, V., Farnsworth, A., Lunt, D.J., Valdes, P., Robson, B.E., Scott, A.C., Lenz, O.K., Naafs, B.D.A., Pancost, R.D., 2017. Mid-latitude continental temperatures through the early Eocene in western Europe. Earth Planet. Sci. Lett. 460, 86–96. https://doi.org/10.1016/j.epsl.2016.12.009

James, N.P., 1997. The Cool-Water Carbonate Depositional Realm. SEPM (Society for Sedimentary Geology), pp. 1–20. https://doi.org/10.2110/pec.97.56.0001

James, N.P., Jones, B., Nelson, C.S., Campbell, H.J., Titjen, J., 2011. Cenozoic temperate and sub-tropical carbonate sedimentation on an oceanic volcano – Chatham Islands, New Zealand. Sedimentology 58, 1007–1029. https://doi.org/10.1111/j.1365-3091.2010.01193.x

Keating-Bitonti, C.R., Ivany, L.C., Affek, H.P., Douglas, P., Samson, S.D., 2011. Warm, not super-hot, temperatures in the early Eocene subtropics. Geology 39, 771–774. https://doi.org/10.1130/G32054.1

Keery, J.S., Holden, P.B., Edwards, N.R., 2018. Sensitivity of the Eocene climate to CO_2 and orbital variability. Clim. Past 14, 215–238. https://doi.org/10.5194/cp-14-215-2018

Kemp, D.W., Oakley, C.A., Thornhill, D.J., Newcomb, L.A., Schmidt, G.W., Fitt, W.K., 2011. Catastrophic mortality on inshore coral reefs of the Florida Keys due to severe low-temperature stress. Glob. Change Biol. 17, 3468–3477. https://doi.org/10.1111/j.1365-2486.2011.02487.x

Kiehl, J., Shields, C.A., 2013. Sensitivity of the Palaeocene–Eocene Thermal Maximum climate to cloud properties. Philos. Trans. R. Soc. Math. Phys. Eng. Sci. 371, 20130093. https://doi.org/10.1098/rsta.2013.0093

King, A.L., Howard, W.R., 2005. $\delta^{18}O$ seasonality of planktonic foraminifera from Southern Ocean sediment traps: Latitudinal gradients and implications for paleoclimate reconstructions. Mar. Micropaleontol. 56, 1–24. https://doi.org/10.1016/j.marmicro.2005.02.008

Langer, M.R., Hottinger, L., 2000. Biogeography of Selected “Larger” Foraminifera. Micropaleontology 46, 105–126.

Liang, J., Russell, J.M., Xie, H., Lupien, R.L., Si, G., Wang, J., Hou, J., Zhang, G., 2019. Vegetation effects on temperature calibrations of branched glycerol dialkyl glycerol tetraether (brGDGTs) in soils. Org. Geochem. 127, 1–11. https://doi.org/10.1016/j.orggeochem.2018.10.010

Lunt, D.J., Dunkley Jones, T., Heinemann, M., Huber, M., LeGrande, A., Winguth, A., Loptson, C., Marotzke, J., Roberts, C.D., Tindall, J., Valdes, P., Winguth, C., 2012. A model–data comparison for a multi-model ensemble of early Eocene atmosphere–ocean simulations: EoMIP. Clim. Past 8, 1717–1736. https://doi.org/10.5194/cp-8-1717-2012

Lunt, D.J., Elderfield, H., Pancost, R., Ridgwell, A., Foster, G.L., Haywood, A., Kiehl, J., Sagoo, N., Shields, C., Stone, E., Valdes, P., 2013. Warm climates of the past—a lesson for the future? Philos. Trans. R. Soc. Math. Phys. Eng. Sci. 371, 20130146. https://doi.org/10.1098/rsta.2013.0146

Lunt, D.J., Farnsworth, A., Loptson, C., Foster, G.L., Markwick, P., O'Brien, C.L., Pancost, R.D., Robinson, S.A., Wrobel, N., 2016. Palaeogeographic controls on climate and proxy interpretation. Clim. Past 12, 1181–1198. https://doi.org/10.5194/cp-12-1181-2016

Lunt, D.J., Huber, M., Anagnostou, E., Baatsen, M.L.J., Caballero, R., DeConto, R., Dijkstra, H.A., Donnadieu, Y., Evans, D., Feng, R., Foster, G.L., Gasson, E., Heydt, A.S. von der, Hollis, C.J., Inglis, G.N., Jones, S.M., Kiehl, J., Kirtland Turner, S., Korty, R.L., Kozdon, R., Krishnan, S., Ladant, J.-B., Langebroek, P., Lear, C.H., LeGrande, A.N., Littler, K., Markwick, P., Otto-Bliesner, B., Pearson, P., Poulsen, C.J., Salzmann, U., Shields, C., Snell, K., Stärz, M., Super, J., Tabor, C., Tierney, J.E., Tourte, G.J.L., Tripati, A., Upchurch, G.R., Wade, B.S., Wing, S.L., Winguth, A.M.E., Wright, N.M., Zachos, J.C., Zeebe, R.E., 2017. The DeepMIP contribution to PMIP4: experimental design for model simulations of the EECO, PETM, and pre-PETM (version 1.0). Geosci. Model Dev. 10, 889–901. https://doi.org/10.5194/gmd-10-889-2017

Michel, J., Borgomano, J., Reijmer, J.J.G., 2018. Heterozoan carbonates: When, where and why? A synthesis on parameters controlling carbonate production and occurrences. Earth-Sci. Rev. 182, 50–67. https://doi.org/10.1016/j.earscirev.2018.05.003

Mutti, M., Hallock, P., 2003. Carbonate systems along nutrient and temperature gradients: some sedimentological and geochemical constraints. Int. J. Earth Sci. 92, 465–475. https://doi.org/10.1007/s00531-003-0350-y

Naafs, B.D.A., Inglis, G.N., Zheng, Y., Amesbury, M.J., Biester, H., Bindler, R., Blewett, J., Burrows, M.A., del Castillo Torres, D., Chambers, F.M., Cohen, A.D., Evershed, R.P., Feakins, S.J., Gałka, M., Gallego-Sala, A., Gandois, L., Gray, D.M., Hatcher, P.G., Honorio Coronado, E.N., Hughes, P.D.M., Huguet, A., Könönen, M., Laggoun-Défarge, F., Lähteenoja, O., Lamentowicz, M., Marchant, R., McClymont, E., Pontevedra-Pombal, X., Ponton, C., Pourmand, A., Rizzuti, A.M., Rochefort, L., Schellekens, J., De Vleeschouwer, F., Pancost, R.D., 2017. Introducing global peat-specific temperature and pH calibrations based on brGDGT bacterial lipids. Geochim. Cosmochim. Acta 208, 285–301. https://doi.org/10.1016/j.gca.2017.01.038

Naafs, B.D.A., Rohrssen, M., Inglis, G.N., Lähteenoja, O., Feakins, S.J., Collinson, M.E., Kennedy, E.M., Singh, P.K., Singh, M.P., Lunt, D.J., Pancost, R.D., 2018. High temperatures in the terrestrial mid-latitudes during the early Palaeogene. Nat. Geosci. 11, 766. https://doi.org/10.1038/s41561-018-0199-0

Nodder, S.D., Northcote, L.C., 2001. Episodic particulate fluxes at southern temperate mid-latitudes (42–45°S) in the Subtropical Front region, east of New Zealand. Deep Sea Res. Part Oceanogr. Res. Pap. 48, 833–864. https://doi.org/10.1016/S0967-0637(00)00062-5

Pancost, R.D., Taylor, K.W.R., Inglis, G.N., Kennedy, E.M., Handley, L., Hollis, C.J., Crouch, E.M., Pross, J., Huber, M., Schouten, S., Pearson, P.N., Morgans, H.E.G., Raine, J.I., 2013. Early Paleogene evolution of terrestrial climate in the SW Pacific, Southern New Zealand. Geochem. Geophys. Geosystems 14, 5413–5429. https://doi.org/10.1002/2013GC004935

Pearson, P.N., Ditchfield, P.W., Singano, J., Harcourt-Brown, K.G., Nicholas, C.J., Olsson, R.K., Shackleton, N.J., Hall, M.A., 2001. Warm tropical sea surface temperatures in the Late Cretaceous and Eocene epochs. Nature 413, 481–487. https://doi.org/10.1038/35097000

Prazeres, M., Roberts, T.E., Pandolfi, J.M., 2017. Variation in sensitivity of large benthic Foraminifera to the combined effects of ocean warming and local impacts. Sci. Rep. 7, 45227. https://doi.org/10.1038/srep45227

Read, J., Francis, J., 1992. Responses of some Southern Hemisphere tree species to a prolonged dark period and their implications for high-latitude Cretaceous and Tertiary floras. Palaeogeogr. Palaeoclimatol. Palaeoecol. 99, 271–290. https://doi.org/10.1016/0031-0182(92)90019-2

Sagoo, N., Valdes, P., Flecker, R., Lauren, J.G., 2013. The Early Eocene equable climate problem: can perturbations of climate model parameters identify possible solutions? Philos. Trans. R. Soc. Math. Phys. Eng. Sci. 371, 20130123. https://doi.org/10.1098/rsta.2013.0123

Scheibner, C., Speijer, R.P., 2008. Late Paleocene–early Eocene Tethyan carbonate platform evolution — A response to long- and short-term paleoclimatic change. Earth-Sci. Rev. 90, 71–102. https://doi.org/10.1016/j.earscirev.2008.07.002

Schlager, W., 2003. Benthic carbonate factories of the Phanerozoic. Int. J. Earth Sci. 92, 445–464. https://doi.org/10.1007/s00531-003-0327-x

Schouten, S., Hopmans, E.C., Sinninghe Damsté, J.S., 2013. The organic geochemistry of glycerol dialkyl glycerol tetraether lipids: A review. Org. Geochem. 54, 19–61. https://doi.org/10.1016/j.orggeochem.2012.09.006

Sinninghe Damsté, J.S., 2016. Spatial heterogeneity of sources of branched tetraethers in shelf systems: The geochemistry of tetraethers in the Berau River delta (Kalimantan, Indonesia). Geochim. Cosmochim. Acta 186, 13–31. https://doi.org/10.1016/j.gca.2016.04.033

Sloan, L.C., Barron, E.J., 1990. Equable climates during Earth history? Geology 18, 489–492. https://doi.org/10.1130/0091-7613(1990)018<0489:ECDEH>2.3.CO;2

Sluijs, A., Schouten, S., Pagani, M., Woltering, M., Brinkhuis, H., Damsté, J.S.S., Dickens, G.R., Huber, M., Reichart, G.-J., Stein, R., Matthiessen, J., Lourens, L.J., Pedentchouk, N., Backman, J., Moran, K., the Expedition 302 Scientists, 2006. Subtropical Arctic Ocean temperatures during the Palaeocene/Eocene thermal maximum. Nature 441, 610–613. https://doi.org/10.1038/nature04668

Stilwell, J.D., 2003. Macropalaeontology of the Trochocyathus-Trematotrochus band (Paleocene/Eocene boundary), Dilwyn Formation, Otway Basin, Victoria. Alcheringa Australas. J. Palaeontol. 27, 245–275. https://doi.org/10.1080/03115510308619107

Tierney, J.E., Sinninghe Damsté, J.S., Pancost, R.D., Sluijs, A., Zachos, J.C., 2017. Eocene temperature gradients. Nat. Geosci. 10, 538–539. https://doi.org/10.1038/ngeo2997

Tierney, J.E., Tingley, M.P., 2014. A Bayesian, spatially-varying calibration model for the TEX_{86} proxy. Geochim. Cosmochim. Acta 127, 83–106. https://doi.org/10.1016/j.gca.2013.11.026

Upchurch, G.R., Kiehl, J., Shields, C., Scherer, J., Scotese, C., 2015. Latitudinal temperature gradients and high-latitude temperatures during the latest Cretaceous: Congruence of geologic data and climate models. Geology 43, 683–686. https://doi.org/10.1130/G36802.1

van Hinsbergen, D.J.J. van, Groot, L.V. de, Schaik, S.J. van, Spakman, W., Bijl, P.K., Sluijs, A., Langereis, C.G., Brinkhuis, H., 2015. A Paleolatitude Calculator for Paleoclimate Studies. PLOS ONE 10, e0126946. https://doi.org/10.1371/journal.pone.0126946

Vérard, C., Hochard, C., Baumgartner, P.O., Stampfli, G.M., Liu, M., 2015. 3D palaeogeographic reconstructions of the Phanerozoic versus sea-level and Sr-ratio variations. J. Palaeogeogr. 4, 64–84. https://doi.org/10.3724/SP.J.1261.2015.00068

Walther, G.-R., Gritti, E.S., Berger, S., Hickler, T., Tang, Z., Sykes, M.T., 2007. Palms tracking climate change. Glob. Ecol. Biogeogr. 16, 801–809. https://doi.org/10.1111/j.1466-8238.2007.00328.x

Wang, M., Zong, Y., Zheng, Z., Man, M., Hu, J., Tian, L., 2018. Utility of brGDGTs as temperature and precipitation proxies in subtropical China. Sci. Rep. 8, 194. https://doi.org/10.1038/s41598-017-17964-0

Figures

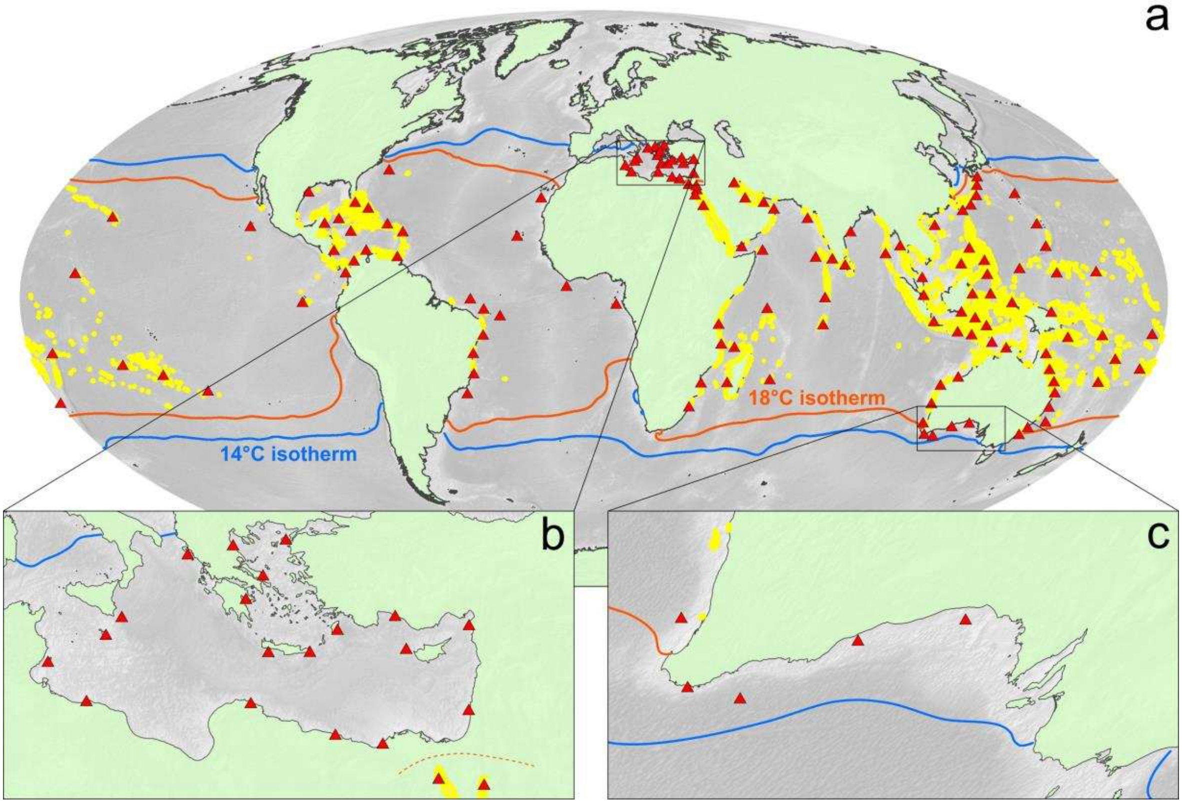

Fig. 1a. Modern global distribution of different photozoan carbonate producers. Yellow polygons are coral reefs, red triangles are large benthic foraminifera (LBF), against the cold month mean 14°C and 18°C sea surface temperature isotherms. Details of areas where LBF occur below the 18°C CMM SST isotherm are shown for the Mediterranean (b) and southern Australia (c).

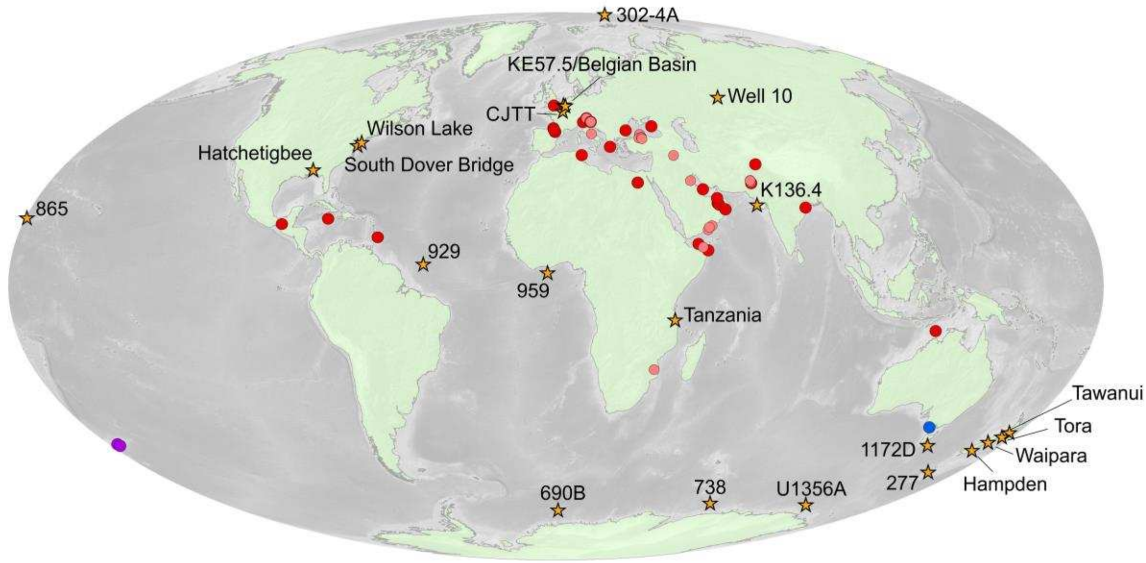

Fig. 2. Modern distribution of EECO quantitative geochemical marine proxies (stars) and Ypresian/Early Eocene photozoans (high confidence red, low confidence pink), heterozoans (dark blue) and mixed assemblages (purple). Data sources outlined in Supplemental files.

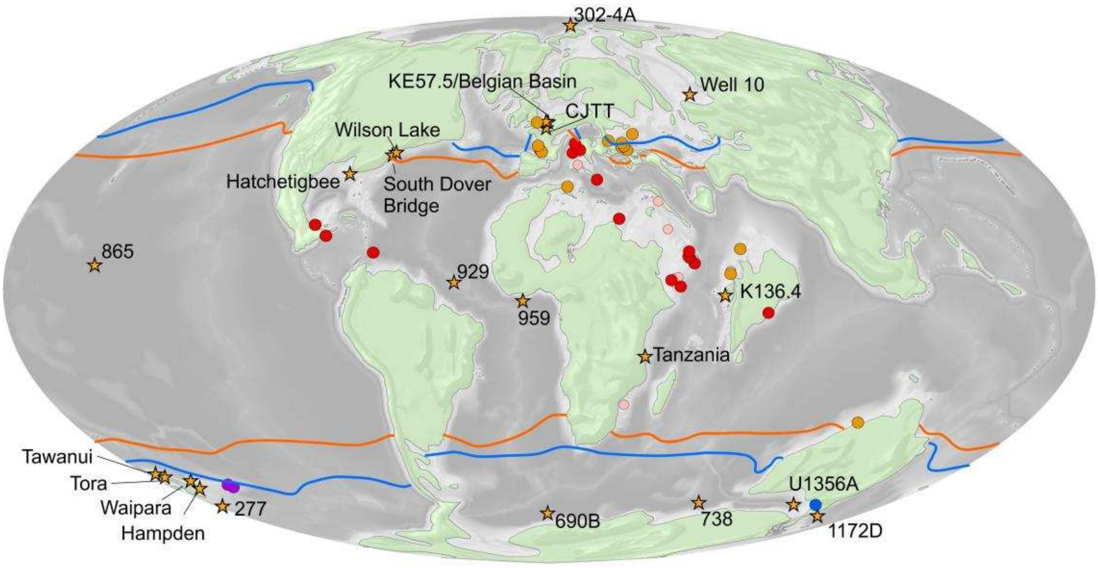

Fig. 3. EECO distribution of photozoan carbonates (red dots = high confidence, and pink = lower confidence), LBF only (orange dots), heterozoans (dark blue) and mixed assemblages (purple) with the HadCM3L simulated 18°C and 14°C CMM SST isotherm (orange and blue lines, respectively). The location of quantitative geochemical proxies is represented by the stars.

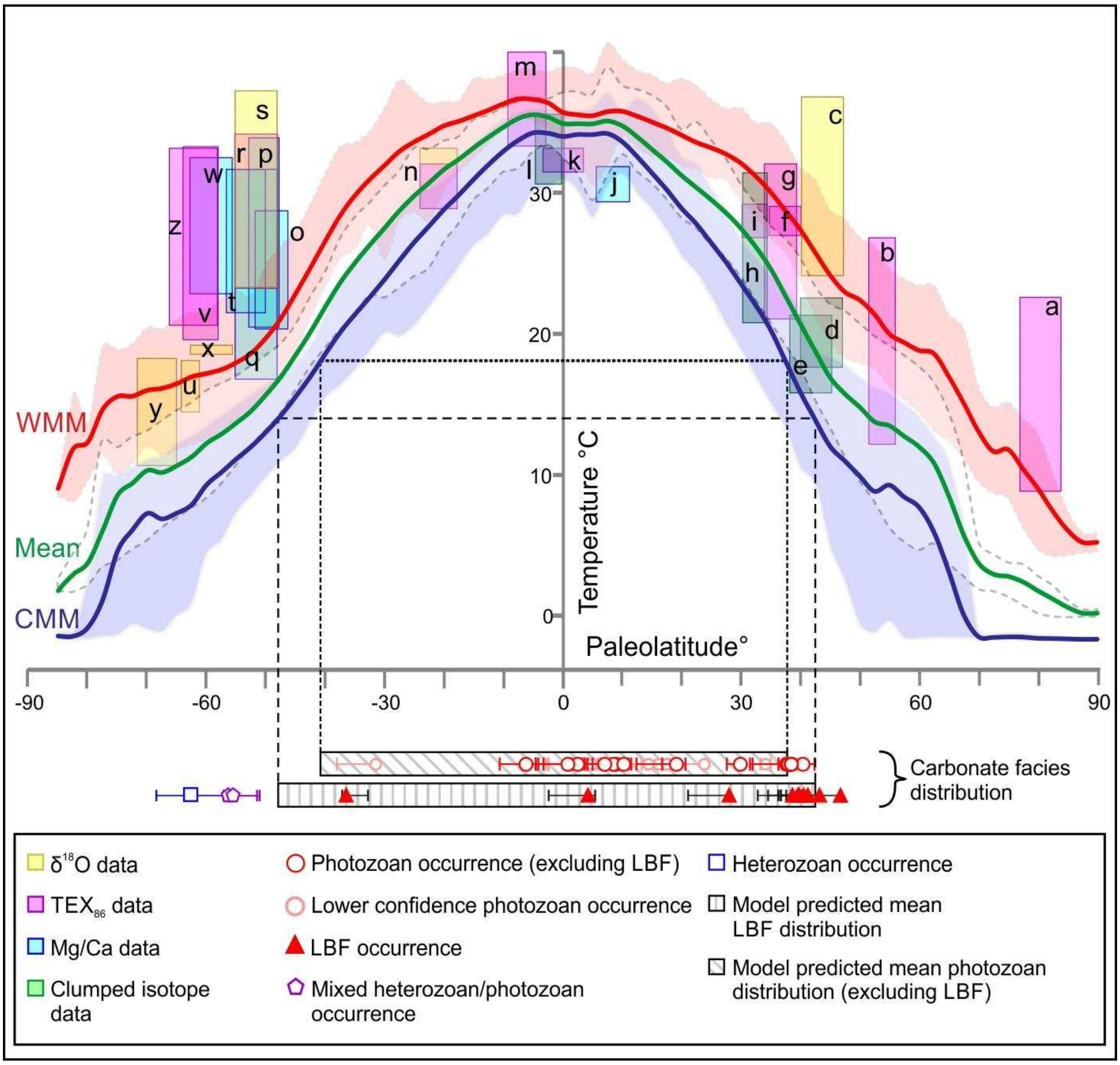

Fig. 4. EECO latitudinal SST profiles for CMM (blue), mean annual (Green) and WMM (red) against the quantitative proxy estimates and the distribution of photozoan, heterozoan and mixed carbonates. The shading around the simulated temperatures represents the zonal minimum and maximum. Paleolatitude error bars for the proxies represent the absolute range of latitudes resulting from 8 different plate tectonic models. Geochemical proxy data are from (a) IODP site 302-4A, (b) Well 10,

(c) Belgian Basin, (d) Kester Borehole, (e) Paris Basin, (f) Wilson Lake, (g) South Dover Bridge, (h, i) Hatchetigbee, (j) ODP 865, (k) ODP 929, (l) Kutch, India, (m) ODP 959, (n) Tanzania drilling project, (o) Tawanui, (p) Tora, (q, r, s) Waipara, (t) Hampden, (u) ODP 738, (v) U1356A, (w, x) DSDP 277, (y) ODP 690, (z) ODP 1172D (see Supplemental files for details)

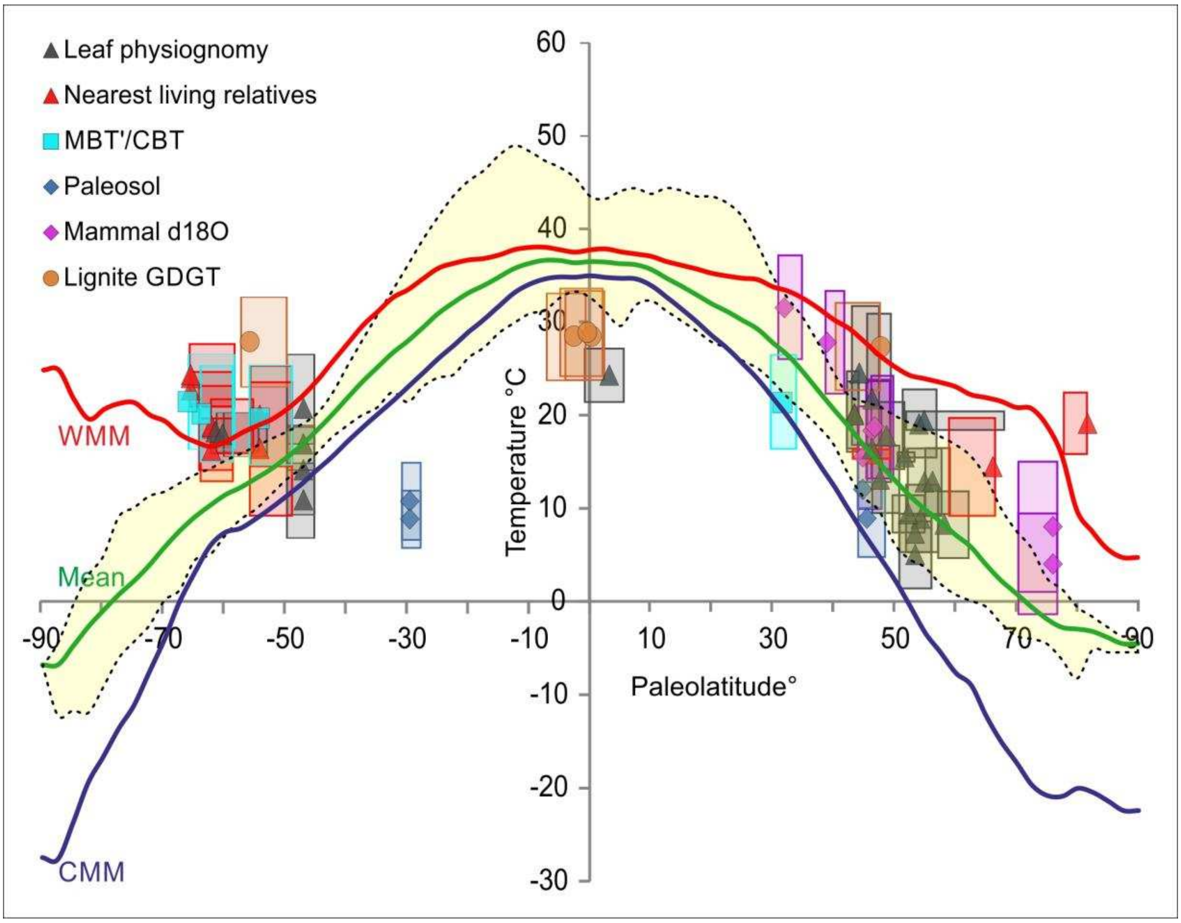

Fig. 5. EECO latitudinal air temperature profiles for CMM (blue), mean annual (green) and WMM (red) against the quantitative proxy estimates. The zonal mean annual temperatures are shown in the yellow shading. Paleolatitude error bars for the proxies represent the absolute range of latitudes resulting from 8 different plate tectonic models. See Supplemental files for details.